Title Page

Development of an oxygen-sensitive degradable peptide probe for the imaging of hypoxia-inducible factor-1–active regions in tumors

Masashi Ueda[1,2], Kei Ogawa[2], Azusa Miyano[2], Masahiro Ono[2], Shinae Kizaka-Kondoh[3], Hideo Saji[2]

[1]Radioisotopes Research Laboratory, Kyoto University Hospital, Faculty of Medicine, Kyoto University, Kyoto 606-8507, Japan

[2]Department of Patho-Functional Bioanalysis, Graduate School of Pharmaceutical Sciences, Kyoto University, Kyoto 606-8501, Japan

[3]Department of Biomolecular Engineering, Graduate School of Bioscience and Biotechnology, Tokyo Institute of Technology, Yokohama 226-8503, Japan

Corresponding author:

Hideo Saji, Ph.D.

Department of Patho-Functional Bioanalysis

Graduate School of Pharmaceutical Sciences

Kyoto University

46-29 Yoshida Shimoadachi-cho, Sakyo-ku, Kyoto 606-8501, Japan

Phone: +81-75-753-4556; Fax: +81-75-753-4568

E-mail: hsaji@pharm.kyoto-u.ac.jp

Running title:

A peptide probe for HIF-1–active tumor imaging

Manuscript category:

Article

Abstract

Purpose

We aimed to develop a radiolabeled peptide probe for the imaging of HIF-1–active tumors.

Procedures

We synthesized the peptide probes that contains or lacks an essential sequence of the oxygen-dependent degradation of HIF-1α in proteasomes ($^{123/125}$I-DKOP30 or ^{125}I-mDKOP, respectively). The degradation of probes was evaluated *in vitro* using cell lysates containing proteasomes. *In vivo* biodistribution study, planar imaging, autoradiography, and comparison between probe accumulation and HIF-1 transcriptional activity were also performed.

Results

The ^{125}I-DKOP30 underwent degradation in a proteasome-dependent manner, while ^{125}I-mDKOP was not degraded. Biodistribution analysis showed ^{125}I-DKOP30 accumulation in tumors. The tumors were clearly visualized by *in vivo* imaging, and intratumoral distribution of ^{125}I-DKOP30 coincided with the HIF-1α–positive hypoxic regions. Tumoral accumulation of ^{125}I-DKOP30 was significantly correlated with HIF-1–dependent luciferase bioluminescence, while that of ^{125}I-mDKOP was not.

Conclusion

^{123}I-DKOP30 is a useful peptide probe for the imaging of HIF-1–active tumors.

Key words:

Tumor hypoxia; Hypoxia-inducible factor-1; Oxygen-dependent degradation; Peptide; Nuclear medical imaging

Introduction

An imbalance between blood supply and the rapid rate of cell growth in solid tumors creates regions of tumor hypoxia. Recently, it has been demonstrated that hypoxic tumor cells acquire active proliferating potency and enhanced metastatic characteristics and furthermore that these regions are closely related to resistance to radiotherapy and chemotherapy [1-3]. The transcription factor hypoxia-inducible factor-1 (HIF-1) is upregulated in tumor hypoxia and plays a major role in tumor progression by activating various genes related to the hypoxic response [4]. Thus, identifying HIF-1–active cells in hypoxic tumor regions can yield valuable information for appropriate cancer therapy.

HIF-1 is a heterodimer that consists of an oxygen-sensitive α subunit (HIF-1α) and the constitutively expressed β subunit (HIF-1β). HIF-1 activity is regulated mainly by degradation of the HIF-1α subunit. In normoxia, HIF-1α is hydroxylated by prolyl hydroxylases (PHDs) on the proline residues in the oxygen-dependent degradation domain (ODD). The hydroxylated proline accelerates the interaction of HIF-1α protein with von Hippel–Lindau tumor suppressor protein (pVHL), resulting in rapid ubiquitination and subsequent degradation of HIF-1α by the proteasome [5, 6]. In hypoxia, HIF-1α evades degradation and is accumulated in large amounts in the nucleus; it turns on the expression of various proteins involved in malignant progression and treatment resistance [7]. In particular, the ODD of HIF-1α is responsible for the regulation of HIF-1 activity.

It is reported that high levels of expression of HIF-1α are observed when the oxygen partial

pressure (pO_2) drops below 40 mmHg [8]. However, different tissues have different thresholds of pO_2 for the stabilization of HIF-1α [9-11]. For example, since pulmonary cells usually exist under relatively high oxygen concentrations, the pO_2 that these cells regard as abnormal is relatively high. On the other hand, bone marrow cells are consistently exposed to low oxygen concentrations and acquire no HIF-1 activity even when they are kept under the same pO_2 as pulmonary cells [12]. Therefore, to visualize the HIF-1–active cells, probes which respond to absolute pO_2 are insufficient compared to probes which contain an ODD and are degraded in a manner similar to HIF-1α.

A chimeric protein probe ($^{123/125}$I-IPOS) that contains an ODD and degrades in the same manner as HIF-1α under normoxic conditions was previously developed in our laboratory. A clear tumor image was obtained at 24 h after the injection of ^{123}I-IPOS, and accumulation of ^{123}I-IPOS in the tumor was found to correlate with HIF-1 activity [13-16]. However, numerous criteria must be met in order to apply a protein probe to clinical use. Therefore, to expand prospective clinical application, the present study aimed to develop a peptide-based imaging probe that is degraded in a manner similar to HIF-1α. Based on the degradation mechanism of HIF-1α, we selected $ODD_{547-574}$ as the basic scaffold for the oxygen-sensitive peptide probe with modified sequences for site-specific radiolabeling and increased membrane permeability, and we evaluated the feasibility of the ODD-based peptide as an imaging probe for HIF-1–active tumor hypoxia.

Experimental Procedures

Materials

The 9-fluorenylmethyloxycarbonyl (Fmoc)-protected amino acids and Fmoc-NH-SAL-PEG Resin were purchased from Watanabe Chemical Industries, Ltd. (Hiroshima, Japan). All of the peptides employed in this study were automatically synthesized by a peptide synthesizer (PSSM-8; Shimadzu Corporation, Kyoto, Japan). Matrix assisted laser desorption/ionization mass spectra (MALDI-MS) were obtained with AXIMA-CFR Plus (Shimadzu Corporation). Reverse-phase high-performance liquid chromatography (HPLC) was performed using a Shimadzu-HPLC-gradient system (LC-20AD; Shimadzu Corporation) equipped with a $5C_{18}$-AR-II column (4.6 mm × 150 mm for analytical HPLC and 10 mm × 250 mm for preparative HPLC, Nacalai Tesque, Inc., Kyoto, Japan). The analytical HPLC was carried out with a linear gradient of 0.1% trifluoroacetic acid (TFA) in acetonitrile and 0.1% aqueous TFA from 1:9 to 7:3 over 30 min, flow rate 1.0 mL/min, detection at 220 nm. Na[^{125}I]I was purchased from PerkinElmer, Inc. (MA, USA). NH_4[^{123}I]I was kindly supplied by Nihon Medi-Physics Co., Ltd. (Tokyo, Japan). 1-(3-[$^{123/125}$I]iodophenyl)maleimide ($^{123/125}$I-IPM) and nonradioactive IPM were prepared according to procedures described previously [17]. Other reagents were of reagent grade and used as received.

Design and Synthesis of Peptides

We designed 5 peptides, shown in Table 1. For site-specific radiolabeling, a glycylcysteine was conjugated to the C-terminal of the $ODD_{547\text{-}574}$ scaffold, and the whole sequence was named

OP30. To increase membrane permeability, the 9 amino acids at the N-terminal of OP30 were replaced by L-lysine or D-lysine, producing the peptides KOP30 and DKOP30, respectively. Furthermore, proline residues in KOP30 and DKOP30 that were essential to oxygen-dependent degradation of the peptides were replaced by L-alanine, producing mKOP and mDKOP, respectively.

All peptides were synthesized by Fmoc-solid-phase peptide synthesis according to the standard protocol of the peptide synthesizer. *N,N′*-diisopropylcarbodiimide/1-hydroxybenzotriazole, and *N,N*-diisopropylethylamine were used as coupling reagents and base, respectively. For removal of Fmoc group, 20% piperidine in *N*-methylpyrrolidone was used. Deprotection of the peptides and cleavage from the resin were simultaneously performed using TFA/ethanedithiol/H_2O/triisopropylsilane (95/2.5/2.5/1, v/v). The crude peptides were purified by preparative HPLC, and their identity was determined by analytical HPLC and MALDI-MS.

OP30: calculated for C150H228N35O51S3 (M+H+); m/z, 3432.55; found, 3432.75.

KOP30: calculated for C160H270N41O44S3 (M+H+); m/z, 3566.93; found, 3567.56.

DKOP30: calculated for C160H270N41O44S3 (M+H+); m/z, 3566.93; found, 3567.37.

mKOP: calculated for C156H266N41O44S3 (M+H+); m/z, 3514.90; found, 3515.42.

mDKOP: calculated for C156H266N41O44S3 (M+H+); m/z, 3514.90; found, 3514.38.

For the conjugation of the peptides and IPM, both were mixed and incubated for 60 min at room temperature. The reaction mixture was purified by HPLC and the identities were determined

by analytical HPLC and MALDI-MS.

OP30-IPM: calculated for C160H234IN36O53S3 (M+H+); m/z, 3731.50; found, 3731.99.

KOP30-IPM: calculated for C170H276IN42O46S3 (M+H+); m/z, 3865.88; found, 3866.05.

DKOP30-IPM: calculated for C170H276IN42O46S3 (M+H+); m/z, 3865.88; found, 3866.43.

mKOP-IPM: calculated for C166H272IN42O46S3 (M+H+); m/z, 3813.84; found, 3813.01.

mDKOP-IPM: calculated for C166H272IN42O46S3 (M+H+); m/z, 3813.84; found, 3813.77.

Radiolabeling

$^{123/125}$I-IPM solution (acetonitrile, 50–150 μL) was added to 50 μL of 0.1 M phosphate buffer (pH 7.0) containing 300 μg of each peptide, and the mixture was incubated at room temperature for 30 min. The reaction mixture was then purified by HPLC (analytical HPLC conditions). The radiochemical yield of each peptide calculated from Na[^{125}I]I as a starting material was approximately 70%. The radiochemical yield of ^{123}I-DKOP30 calculated from NH_4[^{123}I]I as a starting material was 24%. The radiochemical purity of all the probes synthesized in this study was >97%. The peptide probes were injected into mice as 0.1% tween80-containing saline solution.

Degradation Assay of Peptide Probes

The degradation of radiolabeled peptides through the ubiquitin proteasome pathway was evaluated using a Fraction II HeLa Degradation Kit (Boston Biochem, Inc., Cambridge, MA, USA)

[18]. According to the manufacturer's protocol, each peptide (75 kBq, 15 μL of 50 mM HEPES buffer, pH 7.6) was incubated with a cell extract containing proteasomes. To determine whether the degradation was proteasome-dependent, a proteasome inhibitor, MG-132 (6.7 μM at final concentration), was used. After 1 h incubation at 37°C, 50 mM HEPES buffer (100 μL) and trichloroacetic acid (30 μL) were added to stop the reaction. The reaction mixture was centrifuged at 10,000 × *g* for 5 min at 4°C (Micro Cooling Centrifuge 1700; Kubota, Osaka, Japan) and the supernatant was filtrated using a 0.45-μm filter (Millipore; Billerica, MA, USA). The filtrate was analyzed by HPLC (analytical HPLC conditions). The eluent was collected every 1 min and radioactivity was measured with an automatic well-type γ-counter (Cobra 2; Packard Instruments, USA). The assay was performed in triplicate.

Cell Culture

HeLa human cervical carcinoma cells were obtained from the American Type Culture Collection and FM3A mouse mammary carcinoma cells were purchased from the Health Science Research Resources Bank. Suit2/Luc human pancreatic carcinoma cells that express luciferase in response to HIF-1 activity were established by Prof. Kizaka-Kondoh [19]. All the cells were maintained in 10% fetal bovine serum-Dulbecco's modified Eagle's medium (DMEM; Nissui Pharmaceutical, Tokyo, Japan). The culture media were supplemented with penicillin (100 units/mL) and streptomycin (100 μg/mL). Cells were incubated at 37°C in a well-humidified

incubator with 5% CO_2 and 95% air for normoxic culture or in an anaerobic chamber (Concept Mini MACS; Biotrace Limited, UK) for hypoxic culture (5% CO_2 and 95% N_2).

Cell Uptake Assay

HeLa cells were incubated in advance for 18 h under either normoxic or hypoxic conditions, after which ^{125}I-OP30, ^{125}I-KOP30, or ^{125}I-DKOP30 (18 kBq, 1 mL of DMEM) was added. The cells then further incubated for 10, 30, 60, and 120 min under normoxic or hypoxic conditions. After incubation, cells were washed 4 times with phosphate-buffered saline and lysed with 0.2 N sodium hydroxide aqueous solution. The radioactivity of the lysate was measured using the γ-counter. The protein concentration was measured with a BCA Protein Assay Kit (Pierce, Rockford, IL, USA) and used for normalization.

Animal Model

Animal studies were conducted in accordance with our institutional guidelines, and the experimental procedures were approved by the Kyoto University Animal Care Committee. Female C3H/He mice and BALB/c nu/nu mice at 5 weeks of age were purchased from Japan SLC, Inc. (Hamamatsu, Japan) and kept at a constant ambient temperature under a 12-h light/dark cycle with free access to food and water. Models of FM3A and Suit2/Luc tumors were prepared as described in previous reports [20, 21]. Approximately 2 weeks after tumor implantation, the mice were subjected

to a tracer study. The average diameter of the tumors was 11 mm.

Biodistribution

^{125}I-KOP30, ^{125}I-DKOP30 or ^{125}I-mDKOP (18 kBq) was injected intravenously into FM3A-implanted mice (n = 3–4). The mice were euthanized at 15, 60, and 120 min after injection. Whole organs were immediately collected and weighed, and the radioactivity was measured. The results were expressed as the percentage injected dose per gram (%ID/g), except for the stomach and neck (%ID). The blood half-life of ^{125}I-DKOP30 was calculated by nonlinear regression analysis using GraphPad Prism 5 (GraphPad Software, Inc., San Diego, CA) according to one-phase exponential decay.

In vivo *Planar Imaging*

^{123}I-DKOP30 (37 MBq) was injected intravenously into FM3A-implanted mice (n = 4). After 2 h, the mice were placed on a scanner bed in the supine position under 2.5% isoflurane anesthesia. Planar images were acquired for 10 min using a SPECT-2000H scanner (Hitachi Medical Corporation, Tokyo, Japan) equipped with a low-energy, high-resolution, parallel-hole collimator [13, 20]. An energy window was set to 160 keV ± 30%. The detector used was only one-head and qualitative images were obtained. The image is shown as a raw image and is not normalized by injected radioactivity.

Autoradiography and Immunohistochemistry

Pimonidazole (PIMO: 60 mg/kg) was injected intraperitoneally into FM3A-implanted mice (n = 3), and 3 h later, ^{125}I-DKOP30 (1.8 MBq) was injected intravenously. At 2 h after ^{125}I-DKOP30 injection, the tumor was removed and frozen in hexane (−80°C). The frozen tumor samples were cut into 20-μm–thick sections and adjacent 10-μm–thick sections. After 4-day exposure of the 20-μm sections to an imaging plate (Fuji Imaging Plate BAS-SR; Fuji Photo Film, Tokyo, Japan), autoradiograms were obtained using a BAS5000 scanner (Fuji Photo Film). The adjacent 10-μm sections were subjected to dual fluorescent immunostaining for HIF-1α and PIMO according to a previously described method [21].

Comparison between Probe Accumulation and HIF-1 Transcriptional Activity

^{125}I-DKOP30 or ^{125}I-mDKOP (25 kBq) was injected intravenously into Suit2/Luc-implanted mice (n = 6). D-luciferin solution (200 μL, 10 mg/mL in saline; VivoGlo Luciferin, Promega, WI, USA) was injected intraperitoneally at 100 min after administration of the radiolabeled probe. After 20 min, the mice were anesthetized with 2.5% isoflurane that was an optimal anesthetic because it had negligible effects on tumor hemodynamics and partial oxygen pressure [22]. Bioluminescence imaging was performed using an IVIS Spectrum System (Xenogen, Alameda, CA, USA). After the bioluminescence imaging, the mice were euthanized and the

radioactivity of the tumors was measured. The bioluminescent signal intensity within the tumors was analyzed using Living Image 3.0 software (Xenogen).

Statistical Analyses

The statistical data among more than 3 groups were assessed by the Kruskal-Wallis test followed by a Bonferroni correction. Comparisons between 2 groups were performed with the Mann-Whitney *U* test. Correlation coefficients were assessed using the Spearman rank analysis. A *P* value of <0.05 was considered statistically significant.

Results

Degradation of Peptide Probes

Typical radio-HPLC chromatograms of assay samples are shown in Fig. 1. The radiochemical purity of each probe before incubation was >95%. After incubation with the cell extract containing proteasomes, all of the probes containing proline residues were degraded. The radioactivity eluted in the intact fraction was 5% ± 1% (^{125}I-OP30), 12% ± 1% (^{125}I-KOP30), and 27% ± 12% (^{125}I-DKOP30). On the other hand, displacement of the proline residues significantly blocked the degradation of the probes, and the radioactivity eluted in the intact fraction was 88% ± 4% (^{125}I-mKOP) and 77% ± 13% (^{125}I-mDKOP). There were significant difference between proline-containing probes (^{125}I-OP30, ^{125}I-KOP30, and ^{125}I-DKOP30) and proline-displaced probes

(^{125}I-mKOP and ^{125}I-mDKOP) ($P < 0.01$). Moreover, the proteasome inhibitor significantly inhibited the degradation of ^{125}I-DKOP30 (intact fraction 75% ± 6%, $P < 0.01$). Values are represented as the mean ± standard deviation of 3 examinations.

Cell Uptake Assay

After 1 h incubation under hypoxic conditions, there was significantly higher accumulation of ^{125}I-KOP30 and ^{125}I-DKOP30 than of ^{125}I-OP30 in the HeLa cells (Fig. 2a; ^{125}I-OP30 0.5% ± 0.1%, ^{125}I-KOP30 48% ± 14%, and ^{125}I-DKOP30 41% ± 6%) ($P < 0.05$). Furthermore, cellular uptake of ^{125}I-KOP30 and ^{125}I-DKOP30 under hypoxic conditions at each time point was at least 3.5-fold greater than that recorded under normoxic conditions (Fig. 2b and c).

Biodistribution

The results of the biodistribution analysis are summarized in Tables 2, 3, and 4. The biodistribution of 3 probes were similar; there was a high level of radioactivity accumulation in the kidneys and a moderate level in blood, liver, and lung at 15 min after injection, and it fell rapidly. Radioactivity in the intestine gradually increased. Radioactivity accumulation in the neck was negligible. Compared to ^{125}I-KOP30, ^{125}I-DKOP30 and ^{125}I-mDKOP showed significant greater retention by the tumor at 60 and 120 min post injection ($P < 0.05$). Among the tumor-to-blood ratios of 3 probes, only ^{125}I-DKOP30 was >1 at 120 min after injection, though the radioactivity

accumulation in blood and tumor was not statistically different.

In vivo *Planar Imaging*

Figure 3 shows the accumulation of ^{123}I-DKOP30 in tumor. Accumulation of ^{123}I-DKOP30 in the abdominal region was high, but there was little accumulation in the thoracic region, and no radioactivity accumulated in the thyroid. These findings were consistent with the data from the biodistribution evaluation.

Autoradiography and Immunohistochemistry

The autoradiogram indicated a heterogeneous distribution of ^{125}I-DKOP30 in the tumor (Fig. 4). Dual fluorescent immunohistochemistry confirmed the presence of HIF-1α- and PIMO-positive hypoxic areas in the tumor. Sections derived from PIMO-untreated mice were not stained with anti-PIMO antibody, and no HIF-1α signal was detected in the negative control antibody-treated sections (data not shown). Although autoradiographic images affected by blur effect and partial volume effect, the majority of ^{125}I-DKOP30-accumulation was in areas that corresponded to the HIF-1α- and PIMO-positive areas (white arrowheads in Fig. 4). However, there were also a few areas where the HIF-1α or PIMO signal was positive, but where ^{125}I-DKOP30 had not accumulated (black arrowheads in Fig. 4).

Comparison between Probe Accumulation and HIF-1 Transcriptional Activity

There was significant positive correlation observed between HIF-1-induced luciferase bioluminescence and ^{125}I-DKOP30 accumulation at 2 h after the injection ($R = 0.72$, $P < 0.01$; Fig. 5a). On the other hand, tumor accumulation of ^{125}I-mDKOP was not significantly correlated with HIF-1 transcriptional activity ($R = 0.35$; Fig. 5b).

Discussion

In the development of the oxygen-sensitive degradable peptide probe, it was necessary to identify a peptide sequence that would essentially be degraded in a manner similar to HIF-1α. There are 3 key steps in the degradation of HIF-1α: (1) hydroxylation of proline residues by PHDs; (2) pVHL binding to hydroxylated proline; and (3) ubiquitination at the lysine residue by E3 ligase with the pVHL acting as the substrate recognition component. Thus, we planned a peptide containing both proline and lysine, as well as amino acid sequences important for interaction with PHDs and pVHL, as the basic scaffold for the oxygen-sensitive peptide probe. There are 3 subtypes of PHD (PHD1–3) and 2 proline residues (P402 and P564) that are targeted for hydroxylation. All of the PHDs can hydroxylate P564, but only PHD1 and PHD2 can hydroxylate P402 [23]. Therefore, we thought a P564-based probe might degrade more easily than a P402-based probe. Jaakkola *et al*. found that $ODD_{556\text{-}574}$ was the minimal domain required for the interaction between pVHL and hydroxylated P564 [24]. In addition, 3 lysine residues (K532, K538, and K547) within the ODD of

HIF-1α have been reported as principal ubiquitin acceptors. Only the removal of all of the lysine residues abolishes the ubiquitination of HIF-1α, whereas individual point mutations of these lysine residues had no effect on ubiquitination [25]. This finding indicates there is no order of priority of ubiquitination in the 3 lysine residues. Thus, we selected $ODD_{547\text{-}574}$ as the basic scaffold for an oxygen-sensitive peptide probe, and introduced a glycylcysteine for site-specific radiolabeling (OP30).

Although OP30 was actually degraded by incubation with HeLa cell lysates, this probe did not demonstrate cellular accumulation. Therefore, the $ODD_{547\text{-}555}$ region was replaced by L- or D-lysine (KOP30 or DKOP30, respectively) to increase cell membrane permeability. Both probes showed cellular accumulation as expected, and were degraded by incubation with the HeLa cell lysates. On the other hand, the proline-replaced probes (mKOP and mDKOP) remained intact during the incubation with the HeLa cell lysates. Furthermore, degradation of DKOP30 was inhibited by the addition of the proteasome inhibitor. Taken together, these results indicated that the proline residue and the proteasome were required for the degradation of DKOP30, similarly to HIF-1α. Interestingly, degradation was independent of the conformation of lysine residue. The low regioselectivity of E3 ligase may explain this finding, as well as previous results. For instance, Paltoglou *et al*. reported that the ubiquitination of HIF-1α occurred even when the lysine residue was moved several amino acids away from the original position [25]. Moreover, it has been reported that an ODD-β-galactosidase fusion protein that contains only $ODD_{557\text{-}574}$ and no lysine

residue at the same original position as HIF-1α is still regulated by oxygen [26]. Several lysine residues in the fused β-galactosidase could be used as surrogate ubiquitin acceptors in the ubiquitination process.

The result of the biodistribution analysis showed high uptake and rapid clearance of ^{125}I-KOP30, ^{125}I-DKOP30, and ^{125}I-mDKOP in the kidneys, indicating that all the probes could be mainly excreted by the kidneys. Although the difference was not statistically significant, the tumor accumulation of ^{125}I-mDKOP was greater than that of ^{125}I-DKOP30. Since only 2 amino acids are different between ^{125}I-DKOP30 and ^{125}I-mDKOP, the pharmacokinetics of both probes would be similar. When delivered to tumors, ^{125}I-DKOP30 was degraded and cleared from normoxic regions but ^{125}I-mDKOP was not degraded. Thus, much radioactivity could be retained in ^{125}I-mDKOP-treated tumor. This finding is consistent with a previous report that the clearance of point-mutated ODD probe was slower than that of non-mutated ODD probe [19]. Tumor accumulation of ^{125}I-DKOP30 was greater than that of ^{125}I-KOP30, resulting in the higher tumor-to-blood and tumor-to-muscle ratios of ^{125}I-DKOP30. Although the detailed reason for this phenomenon is not yet known, the finding was consistent with a previous result showing that D-forms of oligoarginines had higher tumor accumulation than L-forms [27]. One reason for this may be the difference in stability, as L-peptides are generally more susceptible than D-peptides to proteolytic enzymes that are independent of HIF-1α regulation. A significant positive correlation between probe accumulation and luciferase signal, i.e., HIF-1 transcriptional activity, was observed

for ^{125}I-DKOP30 but not ^{125}I-mDKOP. The autoradiogram showed heterogeneous distribution of ^{125}I-DKOP30, and a majority of the ^{125}I-DKOP30 accumulated in areas that corresponded to HIF-1α- and PIMO-positive areas. Thus, the accumulation of ^{125}I-DKOP30 would reflect the expression of HIF-1. Because the expression of HIF-1 has been reported to be associated with a poor prognosis in breast, lung, and head and neck cancers [28-30], ^{123}I-DKOP30 could prove useful for detecting HIF-1 activity in those tumors.

The ^{125}I-DKOP30 probe had better pharmacokinetics compared to ^{125}I-IPOS, the oxygen-sensitive degradable protein probe. Protein probes often exhibit slow clearance from the blood, which can impose a long wait to obtain a clear tumor image. ^{125}I-IPOS has shown a blood half-life of 2.2 h [13], while that of the ^{125}I-DKOP30 was 0.6 h. Moreover, the accumulation of ^{125}I-DKOP30 in reticuloendothelial tissues, i.e., liver and spleen, was much lower than that previously reported at 24 h after injection of ^{125}I-IPOS [13]. Thus, ^{125}I-DKOP30 demonstrated rapid clearance from the circulation and lower background radioactivity in the abdominal organs. Accumulation of ^{125}I-DKOP30 in tumor at 2 h after injection was 1.68% ID/g, which was comparable to the data obtained 24 h after injection of ^{125}I-IPOS (1.37% ID/g). However, the tumor-to-blood ratio of ^{125}I-DKOP30 was inferior to that of ^{125}I-IPOS. This may be attributed to the short period of intracellular retention of the cell penetrating peptides [31]. For further improvement of the tumor-to-blood ratio, continued modification to increase intracellular retention of ^{125}I-DKOP30 will be required.

There are 3 isoforms in HIF-α family (HIF-1α, HIF-2α and HIF-3α). Although HIF-3α lacks the C-terminal transactivation domain, HIF-1α and HIF-2α have 48% amino acid sequence identity and similar protein structures. Both proteins have the ODD and proline residues in the ODD are hydroxylated under normoxic conditions, triggering oxygen-dependent degradation of HIF-1α and HIF-2α [32]. Since ^{125}I-DKOP30 is a probe in principle to evaluate the enzyme activity involved in the degradation of HIF-1α as a surrogate marker of the amount of HIF-1α, it could accumulate not only in HIF-1–active but also HIF-2–active regions. In addition that HIF-1 and HIF-2 regulate the expression of many of the same hypoxia-induced genes, each HIF also has unique target genes [4]. HIF-1 and HIF-2 play divergent but complementary roles during the hypoxic response. Although many manuscripts describe the importance of individual isoform involved in tumor, inflammation, development, etc., it is still unclear that one is more important than the other and needs to be investigated. Thus, it has yet unknown whether an isoform-specific imaging probe is required or a pan-HIF imaging probe is enough.

Conclusion

In the present study, we designed and synthesized a peptide-based imaging probe, $^{123/125}$I-DKOP30, based on the degradation mechanism of HIF-1α, in order to visualize HIF-1–active tumors. ^{125}I-DKOP30 was degraded in a proteasome-dependent manner and was highly accumulation in hypoxic cells. *In vivo* tumor imaging was successful and tumoral accumulation of

^{123}I-DKOP30 correlated with HIF-1 activity. The negative-control probe neither degraded *in vitro* nor reflected HIF-1 activity *in vivo*. These findings indicate that ^{123}I-DKOP30 is a useful probe for imaging HIF-1–active tumors. To our knowledge, this is the first report of a peptide-based imaging probe targeting HIF-1–active hypoxic tumors.

Acknowledgments

The authors would like to thank Nihon Medi-Physics Co. Ltd. for providing ammonium [^{123}I]iodide. This work was supported in part by the Research and Development Project on Molecular Probes for Detection of Biological Features on Cancer of the New Energy and Industrial Technology Development Organization (NEDO), Japan, and a Grant-in-Aid for Young Scientists (B) (KAKENHI Grant Number 23791412) from the Japan Society for the Promotion of Science.

Conflict of Interest

The authors declare that they have no conflict of interest.

References

1. Harada H (2011) How can we overcome tumor hypoxia in radiation therapy? J Radiat Res 52:545-556

2. Ogawa K, Chiba I, Morioka T et al (2011) Clinical significance of HIF-1alpha expression in patients with esophageal cancer treated with concurrent chemoradiotherapy. Anticancer Res 31:2351-2359

3. Rohwer N, Cramer T (2011) Hypoxia-mediated drug resistance: novel insights on the functional interaction of HIFs and cell death pathways. Drug Resist Updat 14:191-201

4. Keith B, Johnson RS, Simon MC (2012) HIF1alpha and HIF2alpha: sibling rivalry in hypoxic tumour growth and progression. Nat Rev Cancer 12:9-22

5. Lu X, Kang Y (2010) Hypoxia and hypoxia-inducible factors: master regulators of metastasis. Clin Cancer Res 16:5928-5935

6. Semenza GL (2011) Oxygen sensing, homeostasis, and disease. N Engl J Med 365:537-547

7. Semenza GL (2012) Hypoxia-inducible factors: mediators of cancer progression and targets for cancer therapy. Trends Pharmacol Sci 33:207-214

8. Semenza GL (2012) Hypoxia-inducible factors in physiology and medicine. Cell 148:399-408

9. Jiang BH, Semenza GL, Bauer C, Marti HH (1996) Hypoxia-inducible factor 1 levels vary exponentially over a physiologically relevant range of O_2 tension. Am J Physiol

271:C1172-1180

10. Stroka DM, Burkhardt T, Desbaillets I et al (2001) HIF-1 is expressed in normoxic tissue and displays an organ-specific regulation under systemic hypoxia. Faseb J 15:2445-2453

11. Brahimi-Horn MC, Pouyssegur J (2007) Oxygen, a source of life and stress. FEBS Lett 581:3582-3591

12. Kizaka-Kondoh S, Tanaka S, Harada H, Hiraoka M (2009) The HIF-1-active microenvironment: an environmental target for cancer therapy. Adv Drug Deliv Rev 61:623-632

13. Kudo T, Ueda M, Kuge Y et al (2009) Imaging of HIF-1-active tumor hypoxia using a protein effectively delivered to and specifically stabilized in HIF-1-active tumor cells. J Nucl Med 50:942-949

14. Ueda M, Kudo T, Mutou Y et al (2011) Evaluation of [^{125}I]IPOS as a molecular imaging probe for hypoxia-inducible factor-1-active regions in a tumor: comparison among single-photon emission computed tomography/X-ray computed tomography imaging, autoradiography, and immunohistochemistry. Cancer Sci 102:2090-2096

15. Fujii H, Yamaguchi M, Inoue K et al (2012) In vivo visualization of heterogeneous intratumoral distribution of hypoxia-inducible factor-1alpha activity by the fusion of high-resolution SPECT and morphological imaging tests. J Biomed Biotechnol 2012:262741

16. Ueda M (2012) Development of a method for high-contrasted nuclear medical imaging of hypoxia-inducible factor-1-active tumor by using a pretargeting approach. Yakugaku Zasshi 132:595-600

17. Khawli LA, van den Abbeele AD, Kassis AI (1992) N-(m-[^{125}I]iodophenyl)maleimide: an agent for high yield radiolabeling of antibodies. Int J Rad Appl Instrum B 19:289-295

18. Driscoll J, Goldberg AL (1990) The proteasome (multicatalytic protease) is a component of the 1500-kDa proteolytic complex which degrades ubiquitin-conjugated proteins. J Biol Chem 265:4789-4792

19. Kuchimaru T, Kadonosono T, Tanaka S et al (2010) In vivo imaging of HIF-active tumors by an oxygen-dependent degradation protein probe with an interchangeable labeling system. PLoS One 5:e15736

20. Ueda M, Kudo T, Kuge Y et al (2010) Rapid detection of hypoxia-inducible factor-1-active tumours: pretargeted imaging with a protein degrading in a mechanism similar to hypoxia-inducible factor-1alpha. Eur J Nucl Med Mol Imaging 37:1566-1574

21. Kudo T, Ueda M, Konishi H et al (2011) PET imaging of hypoxia-inducible factor-1-active tumor cells with pretargeted oxygen-dependent degradable streptavidin and a novel 18F-labeled biotin derivative. Mol Imaging Biol 13:1003-1010

22. Baudelet C, Gallez B (2004) Effect of anesthesia on the signal intensity in tumors using BOLD-MRI: comparison with flow measurements by Laser Doppler flowmetry and

oxygen measurements by luminescence-based probes. Magn Reson Imaging 22:905-912

23. Semenza GL (2001) HIF-1, O_2, and the 3 PHDs: how animal cells signal hypoxia to the nucleus. Cell 107:1-3

24. Jaakkola P, Mole DR, Tian YM et al (2001) Targeting of HIF-alpha to the von Hippel-Lindau ubiquitylation complex by O_2-regulated prolyl hydroxylation. Science 292:468-472

25. Paltoglou S, Roberts BJ (2007) HIF-1alpha and EPAS ubiquitination mediated by the VHL tumour suppressor involves flexibility in the ubiquitination mechanism, similar to other RING E3 ligases. Oncogene 26:604-609

26. Harada H, Hiraoka M, Kizaka-Kondoh S (2002) Antitumor effect of TAT-oxygen-dependent degradation-caspase-3 fusion protein specifically stabilized and activated in hypoxic tumor cells. Cancer Res 62:2013-2018

27. Nakase I, Konishi Y, Ueda M, Saji H, Futaki S (2012) Accumulation of arginine-rich cell-penetrating peptides in tumors and the potential for anticancer drug delivery in vivo. J Control Release 159:181-188

28. Dales JP, Garcia S, Meunier-Carpentier S et al (2005) Overexpression of hypoxia-inducible factor HIF-1alpha predicts early relapse in breast cancer: retrospective study in a series of 745 patients. Int J Cancer 116:734-739

29. Park S, Ha SY, Cho HY et al (2011) Prognostic implications of hypoxia-inducible

factor-1alpha in epidermal growth factor receptor-negative non-small cell lung cancer. Lung Cancer 72:100-107

30. Eckert AW, Lautner MH, Schutze A et al (2011) Coexpression of hypoxia-inducible factor-1alpha and glucose transporter-1 is associated with poor prognosis in oral squamous cell carcinoma patients. Histopathology 58:1136-1147

31. Kersemans V, Kersemans K, Cornelissen B (2008) Cell penetrating peptides for in vivo molecular imaging applications. Curr Pharm Des 14:2415-2447

32. Koh MY, Powis G (2012) Passing the baton: the HIF switch. Trends Biochem Sci 37:364-372

Table 1. Peptides synthesized in this study

Name	Amino acid sequence
OP30	H-KNPFSTQDTDLDLEMLAPYIPMDDDFQLGC-NH_2
KOP30	H-KKKKKKKKKDLDLEMLAPYIPMDDDFQLGC-NH_2
mKOP	H-KKKKKKKKKDLDLEMLAAYIAMDDDFQLGC-NH_2
DKOP30	H-<u>KKKKKKKKK</u>DLDLEMLAPYIPMDDDFQLGC-NH_2
mDKOP	H-<u>KKKKKKKKK</u>DLDLEMLAAYIAMDDDFQLGC-NH_2

The underlined letters represent D-amino acids.

Table 2. Biodistribution of ^{125}I-KOP30 in FM3A-implanted mice

	Time after injection (min)		
Organ	15	60	120
Blood	9.40± 1.18	1.89 ± 0.17	1.04 ± 0.14
Spleen	3.80 ± 0.45	0.72 ± 0.07	0.36 ± 0.11
Pancreas	4.38 ± 0.39	1.41 ± 0.15	0.91 ± 0.28
Intestine	6.23 ± 0.64	8.82 ± 0.30	10.88 ± 4.12
Liver	13.53 ± 7.38	5.37 ± 1.15	2.33 ± 0.57
Kidney	80.54 ± 17.25	9.62 ± 0.33	2.66 ± 0.07
Stomach	0.76 ± 0.09	0.49 ± 0.12	0.72 ± 0.20
Heart	5.43 ± 0.90	1.33 ± 0.26	0.46 ± 0.16
Lung	8.84 ± 1.11	1.81 ± 0.29	1.03 ± 0.26
Tumor	3.51 ± 0.74	1.41 ± 0.11	0.73 ± 0.16
Muscle	3.08 ± 0.39	0.70 ± 0.20	0.37 ± 0.12
Neck	0.09 ± 0.02	0.05 ± 0.00	0.02 ± 0.01
Tumor/blood	0.37 ± 0.05	0.75 ± 0.12	0.71 ± 0.14
Tumor/muscle	1.13 ± 0.11	2.17 ± 0.79	2.08 ± 0.59

Organ uptake values are expressed as the percent injected dose per gram of tissue, except in the case of the stomach and the neck (percent injected dose).

Values are represented as the mean ± S.D., $n = 3$.

Table 3. Biodistribution of ^{125}I-DKOP30 in FM3A-implanted mice

	Time after injection (min)		
Organ	15	60	120
Blood	8.88 ± 1.02	3.15 ± 0.19	1.53 ± 0.30
Spleen	3.85 ± 0.56	1.08 ± 0.13	0.50 ± 0.11
Pancreas	3.14 ± 0.21	1.46 ± 0.20	0.54 ± 0.15
Intestine	4.67 ± 0.37	6.43 ± 1.13	8.05 ± 1.78
Liver	15.59 ± 1.18	5.77 ± 0.65	3.26 ± 0.51
Kidney	71.05 ± 13.41	17.32 ± 1.54	6.69 ± 0.49
Stomach	0.70 ± 0.07	0.73 ± 0.09	0.93 ± 0.51
Heart	5.44 ± 0.90	1.68 ± 0.13	0.68 ± 0.13
Lung	8.27 ± 1.33	3.32 ± 0.05	1.51 ± 0.21
Tumor	3.96 ± 0.75	2.48 ± 0.18	1.68 ± 0.42
Muscle	2.47 ± 0.45	0.97 ± 0.23	0.43 ± 0.12
Neck	0.09 ± 0.02	0.07 ± 0.01	0.07 ± 0.01
Tumor/blood	0.44 ± 0.04	0.79 ± 0.03	1.11 ± 0.19
Tumor/muscle	1.61 ± 0.25	2.70 ± 0.75	4.12 ± 1.21

Organ uptake values are expressed as the percent injected dose per gram of tissue, except in the case of the stomach and the neck (percent injected dose).

Values are represented as the mean ± S.D., $n = 4$.

Table 4. Biodistribution of ^{125}I-mDKOP in FM3A-implanted mice

	Time after injection (min)		
Organ	15	60	120
Blood	11.84 ± 1.54	5.24 ± 0.04	2.40 ± 0.18
Spleen	4.85 ± 1.29	1.91 ± 0.38	0.75 ± 0.06
Pancreas	2.89 ± 0.29	1.48 ± 0.08	0.79 ± 0.10
Intestine	3.80 ± 0.45	5.82 ± 0.64	7.29 ± 2.34
Liver	17.71 ± 1.68	7.23 ± 0.49	2.80 ± 0.12
Kidney	43.57 ± 3.17	18.31 ± 1.45	5.46 ± 0.16
Stomach	0.91 ± 0.36	0.62 ± 0.17	0.95 ± 0.55
Heart	7.61 ± 0.93	2.76 ± 0.12	0.99 ± 0.10
Lung	10.32 ± 1.21	4.64 ± 0.26	1.91 ± 0.16
Tumor	3.97 ± 0.76	3.23 ± 0.73	1.96 ± 0.11
Muscle	2.10 ± 0.33	1.64 ± 1.22	0.42 ± 0.09
Neck	0.06 ± 0.02	0.12 ± 0.04	0.07 ± 0.01
Tumor/blood	0.34 ± 0.06	0.62 ± 0.14	0.82 ± 0.10
Tumor/muscle	1.89 ± 0.29	2.41 ± 0.80	4.79 ± 1.01

Organ uptake values are expressed as the percent injected dose per gram of tissue, except in the case of the stomach and the neck (percent injected dose).

Values are represented as the mean ± S.D., $n = 4$.

Figure 1

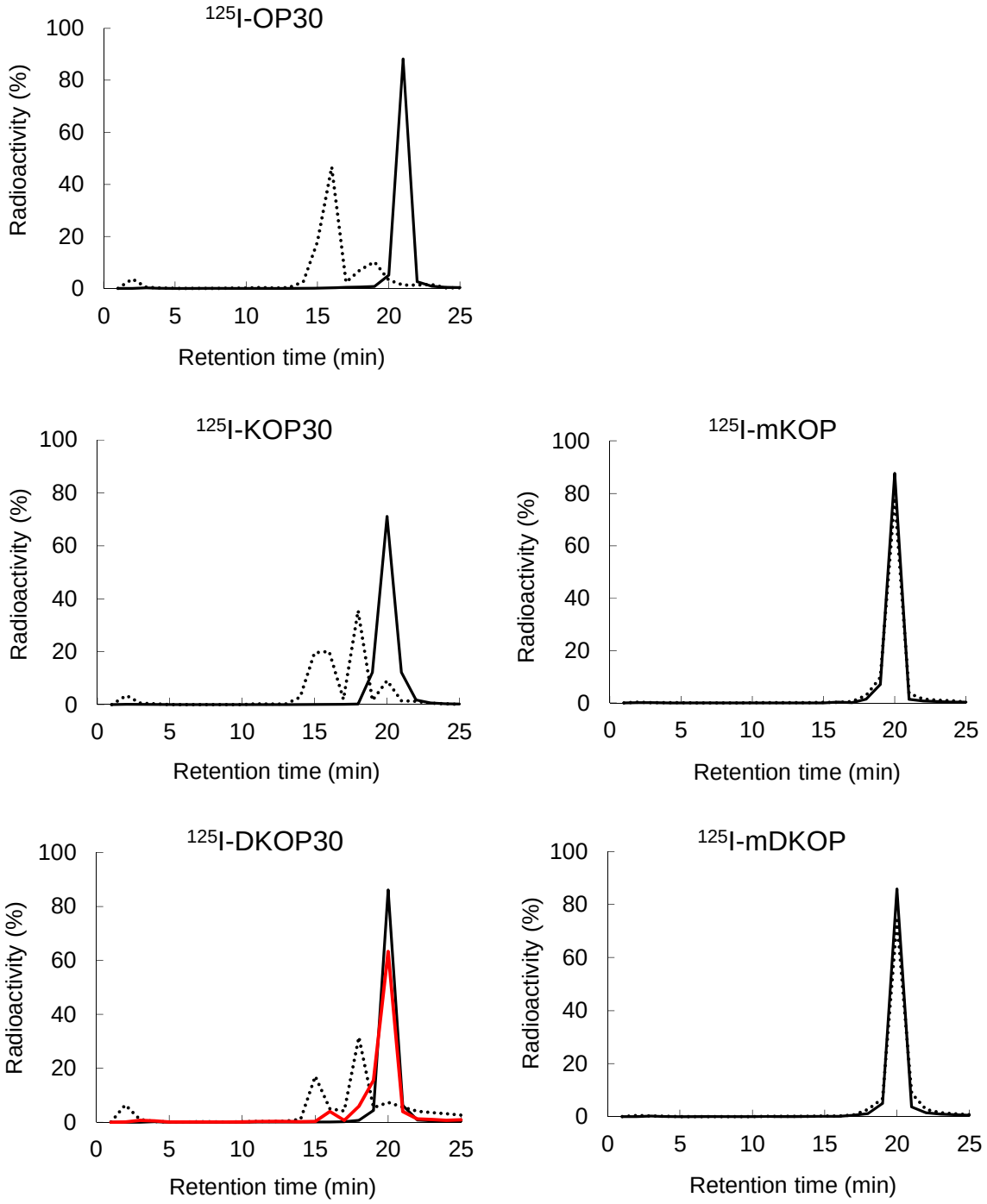

Radio-HPLC chromatograms of each probe before (black solid lines) and after (black dotted lines) incubation with the HeLa cell extract. The proteasome inhibitor MG-132 inhibited the degradation of ^{125}I-DKOP30 (red solid line).

Figure 2

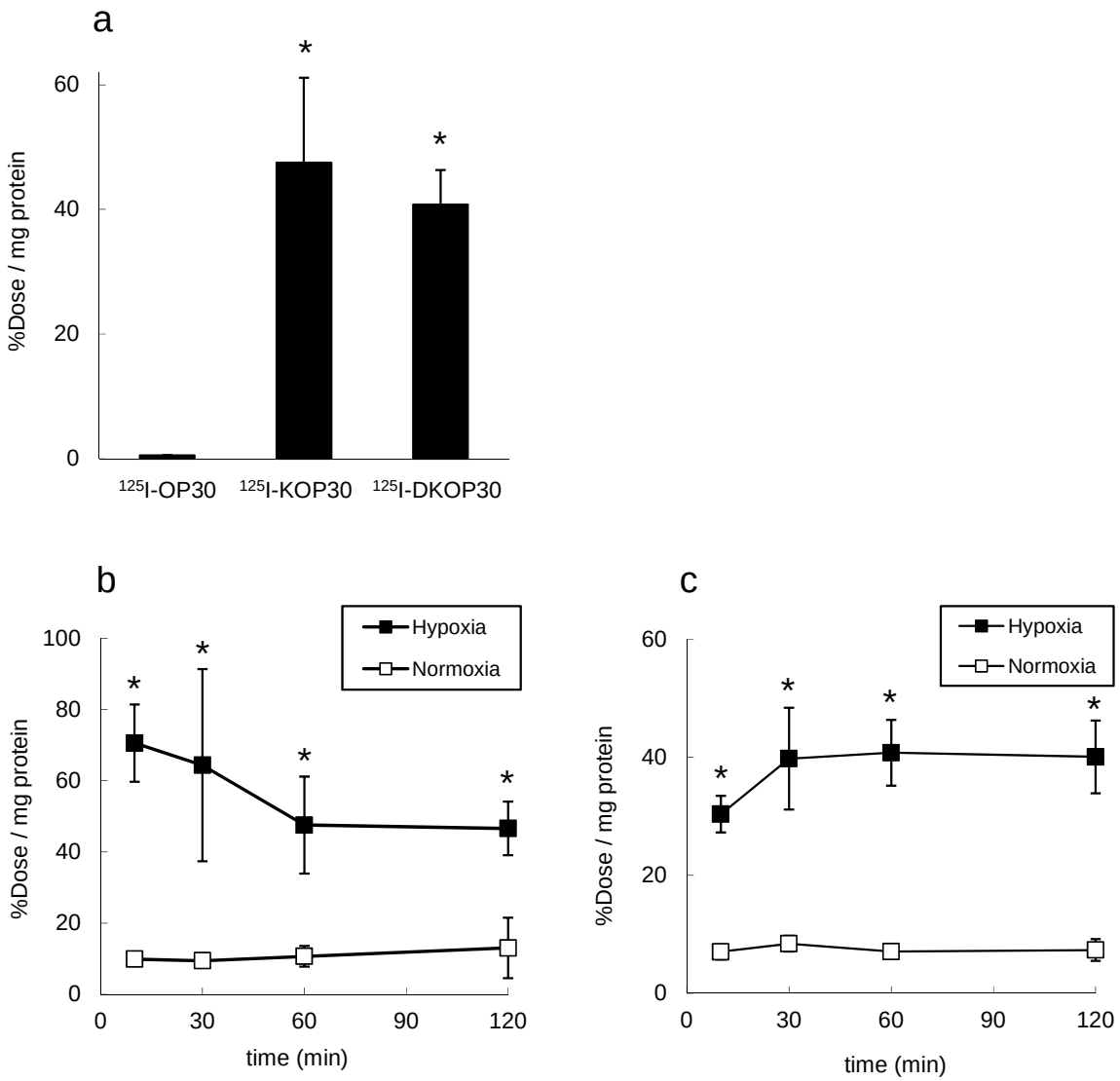

(a) Intracellular radioactivity in HeLa cells after 60 min incubation under hypoxic conditions. Each column represents an average of 3 measurements and each error bar represents the standard deviation (*$P < 0.05$ vs. ^{125}I-OP30). (b, c) Time course of intracellular radioactivity in HeLa cells incubated with ^{125}I-KOP30 (b) or ^{125}I-DKOP30 (c) under either normoxic or hypoxic conditions. Each data point represents an average of 3 measurements and each error bar represents the standard deviation (*$P < 0.05$ vs. normoxia).

Figure 3

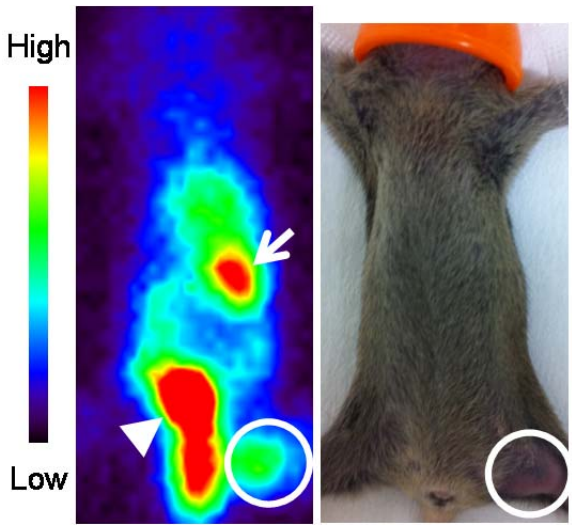

A representative planar image of a FM3A-implanted mouse at 2 h after injection of ^{123}I-DKOP30. The tumor was clearly visualized in the image (*circle*). The gall bladder (*arrow*) and bladder (*arrowhead*) were also visible. Four mice were used in this study.

Figure 4

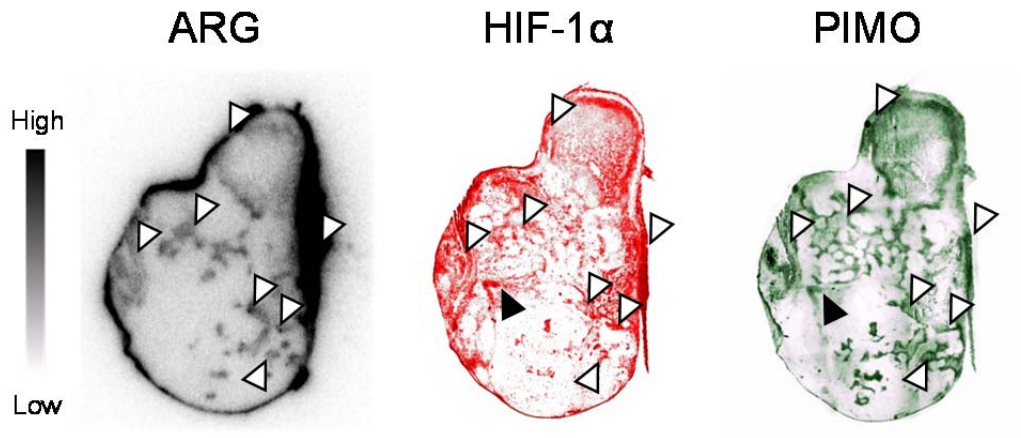

Representative images of an autoradiogram (ARG) of ^{125}I-DKOP30, HIF-1α immunostaining, and pimonidazole (PIMO) immunostaining. The white arrowheads show areas in which any signals were positive, while black arrowheads show the areas in which a discrepancy was observed between ^{125}I-DKOP30 accumulation and immunostaining. Three mice were used in this study.

Figure 5

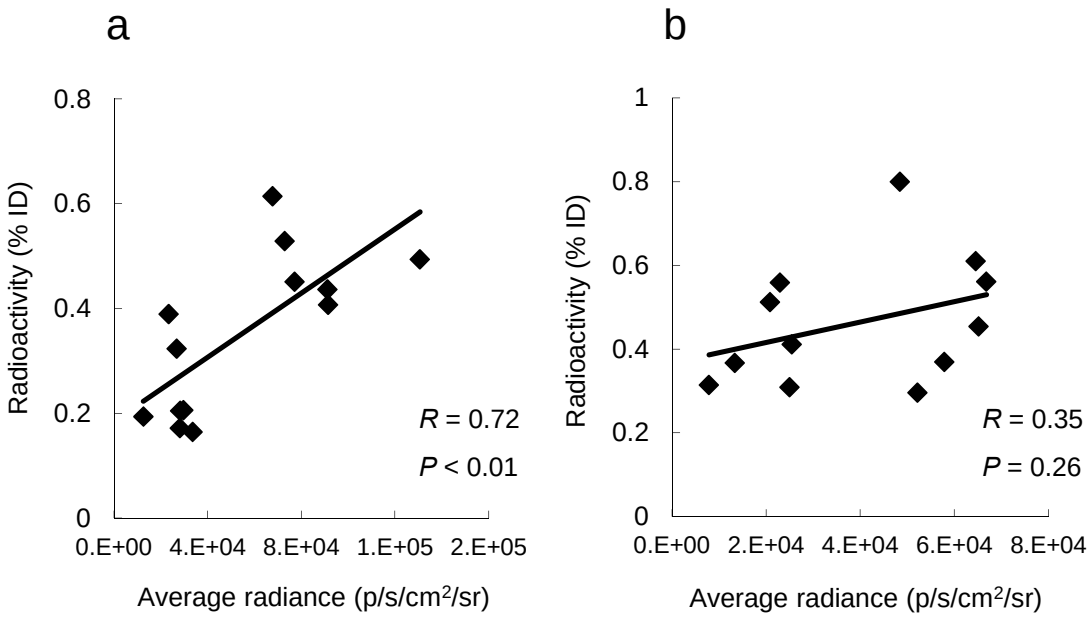

Correlation between HIF-1-dependent luciferase activity and ^{125}I-DKOP30 (a) or ^{125}I-mDKOP (b) accumulation in tumors. Y-axes indicate the accumulated radioactivity of probes and x-axes represent tumor bioluminescence intensity. The correlation coefficient (R) in (a) was 0.72, indicating highly significant correlation between the 2 parameters ($P < 0.01$).